Measurement of the branching fractions of the τ lepton using a tagged sample of τ decays

P. R. Burchat,[a] G. J. Feldman, T. Barklow, A. M. Boyarski, D. L. Burke, J. M. Dorfan, L. Gladney,[b] G. Hanson, K. Hayes, R. J. Hollebeek,[b] W. R. Innes, J. A. Jaros, D. Karlen, A. J. Lankford, R. R. Larsen, B. W. LeClaire, N. S. Lockyer,[b] V. Lüth, C. Matteuzzi,[c] R. A. Ong, M. L. Perl, B. Richter, K. Riles, M. C. Ross, J. M. Yelton,[d] and C. Zaiser
Stanford Linear Accelerator Center, Stanford University, Stanford, California 94305

G. S. Abrams, D. Amidei,[e] A. R. Baden, J. Boyer, F. Butler, G. Gidal, M. S. Gold, G. Goldhaber, L. Golding,[f] J. Haggerty, D. Herrup, I. Juricic, J. A. Kadyk, M. E. Nelson,[g] P. C. Rowson,[h] H. Schellman,[e] W. B. Schmidke, P. D. Sheldon, G. H. Trilling, C. de la Vaissiere,[i] and D. R. Wood
Lawrence Berkeley Laboratory and Department of Physics, University of California, Berkeley, California 94720

M. E. Levi[j] and T. Schaad[k]
Department of Physics, Harvard University, Cambridge, Massachusetts 02138
(Received 29 July 1986)

The branching fractions for the major decay modes of the τ lepton are measured from a sample of tagged τ decays selected from $\tau^+\tau^-$ pairs produced in e^+e^- annihilation. The decay products of one member of the $\tau^+\tau^-$ pair are used to identify the event. The opposite member of the pair is then included in the sample if it satisfies an invariant-mass cut and a charged-multiplicity cut. In this way, we attempt to select an unbiased sample of τ decays. The sample is divided into categories based on charged- and neutral-particle multiplicities, and charged-particle identification. The branching fractions are measured simultaneously, with an unfold technique and a maximum-likelihood fit, with the sum of the branching fractions constrained to be unity. The branching fractions for the decay modes $\tau^-\to\nu_\tau K^-$ and $\tau^-\to\nu_\tau K^{*-}$ are fixed at the world averages in the fit. The following branching fractions are measured: $B(\tau^-\to\nu_\tau e^-\bar{\nu}_e)=(19.1\pm0.8\pm1.1)\%$, $B(\tau^-\to\nu_\tau\mu^-\bar{\nu}_\mu)=(18.3\pm0.9\pm0.8)\%$, $B(\tau^-\to\nu_\tau\pi^-)=(10.0\pm1.1\pm1.4)\%$, $B(\tau^-\to\nu_\tau\pi^-\pi^0)=(25.8\pm1.7\pm2.5)\%$, $B(\tau^-\to\nu_\tau\pi^-(n\pi^0,n>1))=(12.0\pm1.4\pm2.5)\%$, $B(\tau^-\to\nu_\tau\pi^-\pi^+\pi^-)=(6.7\pm0.8\pm0.9)\%$, and $B(\tau^-\to\nu_\tau\pi^-\pi^+\pi^-(n\pi^0,n>0))=(6.1\pm0.8\pm0.9)\%$. The total branching fraction to one charged pion plus at least one neutral hadron is measured to be $(37.8\pm1.2\pm1.0)\%$. Limits on allowed decay modes involving the η meson are discussed.

I. INTRODUCTION

The production and decay of the τ lepton has been extensively studied at e^+e^- storage rings. Measurements of the total cross section, differential cross section, lifetime, and ratios of branching fractions agree well with the standard model. However, the sum of experimentally measured *exclusive* branching fractions to final states containing one charged particle is significantly smaller than the measured *inclusive* branching fraction to final states containing one charged particle.[1] The size of the discrepancy is about $(9\pm2)\%$ (Ref. 2). Either the measured branching fractions are incorrect or there exist significant decay modes for which the exclusive branching fractions have not been measured.

In this analysis the branching fractions for all major decay modes of the τ are measured simultaneously with the sum of the branching fractions constrained to be unity. The measurement is based on a sample of τ decays selected from 207 pb^{-1} of data accumulated with the Mark II detector at the SLAC e^+e^- storage ring operating at a center-of-mass energy of 29 GeV. τ-pair events are identified from the decay products of one of the produced τ leptons with the opposite member of the pair then included in the sample of τ-decay candidates.[3] The sample is divided into subgroups according to charged- and neutral-particle multiplicity, and charged-particle identification. The branching fractions are then measured by means of an unfold technique and a maximum-likelihood fit.

In Sec. II, the Mark II detector is briefly described. The event selection is presented in Sec. III. In Sec. IV, the unfold technique is described and the checks on the Monte Carlo–generated unfold matrix are discussed. The backgrounds are estimated in Sec. V and the results are presented in Sec. VI. In Appendix A, we estimate limits on the branching fractions for allowed decay modes involving the η meson.

II. APPARATUS AND DATA ACQUISITION

The data sample for our measurement was accumulated with the Mark II detector[4] at the e^+e^- storage ring PEP at the Stanford Linear Accelerator Center. The detector is shown in Fig. 1 and the components pertinent to this measurement are described briefly below.

Multilayer cylindrical drift chambers in a 2.3-kG

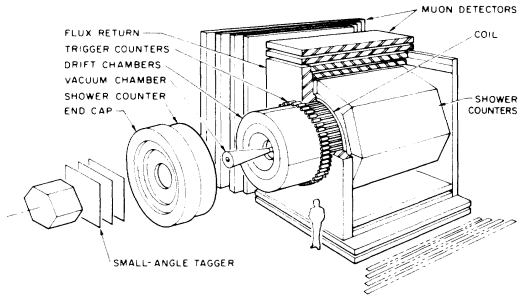

FIG. 1. Isometric view of the Mark II detector.

solenoidal magnetic field measure charged-particle momenta with a resolution of $\sigma_p/p=[(0.02)^2+(0.01p)^2]^{1/2}$ where p is the momentum in GeV/c. The drift-chamber system consists of an inner high-resolution drift chamber with seven concentric layers of sense wires and an outer drift chamber with 16 layers of sense wires, six of which are parallel to the beam pipe and ten of which are rotated by about $\pm 3°$ to determine the momentum component along the beam axis.

Time-of-flight (TOF) scintillation counters at a radius of 1.5 m measure flight times with a resolution of ≈ 320 ps for particles with $|\cos\theta|<0.76$ where θ is the angle between the track and the electron beam. The TOF system is part of the charged-particle trigger and is also used to reject cosmic rays.

Eight lead—liquid-argon (LA) calorimeter modules covering 65% of the solid angle detect electromagnetic showers with an energy resolution of $\sigma_E/E=0.14E^{-1/2}$ where E is the energy in GeV. Each module consists of 37 layers of 2-mm-thick lead separated by 3-mm liquid-argon gaps. The lead layers are alternately ground planes and ionization collecting high-voltage strips which provide spatial information. Some of the readout strips in the same position in different layers are ganged together to reduce the number of readout layers in depth from 18 to 6.

End-cap shower counters consisting of two layers of lead sheets and proportional chambers cover the polar region between approximately 15° and 30°. The energy resolution for photons and electrons is $\sigma_E/E=0.50E^{-1/2}$ where E is the energy in GeV.

Four walls of alternating layers of iron hadron absorber and proportional tubes provide muon identification over 45% of the solid angle. Each wall consists of 1 m of iron and four layers of proportional tubes. The minimum momentum required for a normally incident muon to penetrate all four layers is about 1.8 GeV/c. The proportional tubes in the inner layer of each wall run perpendicular to the beam axis and thus provide spatial information for the polar angle θ. The tubes in the outer three layers run parallel to the beam axis and thus provide spatial information for the azimuthal angle ϕ.

The detector is triggered by various combinations of charged particles and/or energy deposited in the calorimeters. All events used in this analysis correspond to the charged-particle trigger which requires at least two charged particles with momenta transverse to the beam axis greater than ≈ 70 MeV/c entering the TOF counters.

III. EVENT SELECTION

We attempt to make an unbiased selection of τ decays by using the decay products of one τ in the pair to tag the event. The opposite τ decay is then included in the sample (called the candidate sample or tagged sample) if it satisfies the appropriate invariant-mass and charged-multiplicity cuts. If the decay products of both τ's pass the criteria for a tag, both are included in the final sample of tagged τ-decay candidates.

Two different tags are used in this analysis to produce two distinct samples of tagged τ-decay candidates. One tag corresponds to a single charged hadron and is referred to as the one-prong tag; the other tag corresponds to three charged particles and is referred to as the three-prong tag. In both tags a limited number of neutral energy clusters is allowed. These tags are described in detail below. The τ-candidate samples corresponding to the two tags have different potential sources of background and slightly different systematic errors. Therefore, they provide an important cross-check on the final results.

A. Overall cuts

We require that the event satisfy the following criteria to reduce the background from beam-pipe or beam-gas events and from two-photon events: (1) $|z_v|\leq 20$ cm where z_v is the vertex position along the beam direction relative to the beam collision point; (2) ≥ 2 charged tracks each with $|\cos\theta|<0.7$; (3) $E_{\rm ch}>E_{\rm beam}/4\approx 3.6$ GeV where $E_{\rm ch}$ is the sum of the energy of all charged tracks in the event and $E_{\rm beam}$ is the beam energy; (4) $E_{\rm tot}>E_{\rm beam}/2\approx 7.2$ GeV where $E_{\rm tot}$ is the sum of the energy of all charged tracks plus the energy deposited in the calorimeters by photons or other neutral particles.

However, the following classes of events are *exempt* from the last two cuts described above: (1) any event containing a track with momentum greater than 1.25 GeV/c and with LA calorimeter information consistent with an electron; (2) any event containing a track with associated hits in at least three levels of the muon system.

B. The one-prong tag

Selection criteria. Each event is divided into two hemispheres by the plane perpendicular to the thrust axis of the event. All charged tracks and all neutral energy clusters with energy greater than 500 MeV deposited in the LA or end-cap calorimeters are used in the calculation of the thrust axis. The one-prong tag corresponds to one hemisphere of the event with the following properties.

(1) The hemisphere contains exactly one charged track which projects into the active volume of the LA calorimeter and the muon system, is identified as definitely *not* being an electron or a muon, and has a momentum below 10 GeV/c and above 2 GeV/c. The electron and muon rejection criteria are described below. The total visible (charged plus neutral) energy in the hemisphere is less than 12 GeV. These criteria reject QED events of

the type $e^+e^- \to e^+e^-(\gamma)$, $e^+e^- \to \mu^+\mu^-(\gamma)$, $e^+e^- \to e^+e^-e^+e^-$, and $e^+e^- \to e^+e^-\mu^+\mu^-$.

(2) The hemisphere contains three or fewer neutral energy clusters with energy greater than 500 MeV. The invariant mass of the charged particle (assumed to be a π) plus neutrals is less than 1.5 GeV/c^2. These criteria reject hadronic events.

The major decay modes of the τ which have the above properties are $\tau^- \to \nu_\tau \rho^-$, $\tau^- \to \nu_\tau \pi^-$, and $\tau^- \to \nu_\tau \pi^- 2\pi^0$ for which the previously measured branching fractions are about 22, 10, and 8 %, respectively. They contribute approximately 53, 31, and 16 %, respectively, to the tag assuming the above branching fractions.

At this point a cut is made on the charged-particle multiplicity and the invariant mass of the charged and neutral particles (assumed to be pions and photons, respectively) in the τ-decay candidate opposite the one-prong tag. Candidates with more than three charged particles or with mass greater than 2.5 GeV/c^2 are rejected. The number of candidates rejected by this latter cut is used to estimate the hadronic background (see Sec. V). The number of τ candidates which pass all of the criteria for the one-prong tag is 1627.

Electron and muon rejection. In this section the criteria used to reject electrons and muons from the one-prong tag are described. A charged track is identified as definitely *not* being an electron if it projects into the active volume of the LA system and has E/p less than 0.5 where E is the energy in the LA system associated with the track and p is the momentum of the track as measured by the drift chambers. The probability that E/p is less than 0.5 is about 90% for pions and about a tenth of a percent for electrons. The electron rejection inefficiency is discussed in more detail in Sec. V.

A track is classified as *not* being a muon if it is expected to penetrate at least three layers of absorber if it is a muon, the projected track trajectory is at least three times the root-mean-squared scattering distance from the edge of the fiducial volume for at least three layers, and it has no associated hits, or has associated hits in the first and/or fourth layer only, within three times the root-mean-squared scattering distance. A hit in the first layer only, for a track with enough momentum to penetrate at least three layers if it is a muon, is often due to hadronic punchthrough. Isolated hits in the last layer are often noise hits from synchrotron radiation reflecting off the walls in the detector hall. The probability for a muon to pass these criteria is about a tenth of a percent and is discussed in more detail in Sec. V.

C. The three-prong tag

Selection criteria. The three-prong tag corresponds to one hemisphere of the event with the following properties.

(1) The hemisphere contains exactly three charged particles with net charge ± 1.

(2) The total visible (charged plus neutral) energy in the hemisphere is less than 14 GeV. (The maximum of the momentum measured by the drift chamber and the energy in the LA calorimeter associated with the track is used for the energy of each charged track.) This provides rejection against radiative QED events.

(3) There are no oppositely charged pairs of tracks in the hemisphere with a small opening angle consistent with the conversion of a photon into an e^+e^- pair. This cut rejects $e^+e^-\gamma$ and $\mu^+\mu^-\gamma$ events in which the photon converts to an e^+e^- pair.

(4) The hemisphere contains two or fewer neutral energy clusters with energy greater than 500 MeV. The invariant mass of the charged particles (assumed to be pions) plus neutrals is less than 1.7 GeV/c^2. These criteria provide rejection against hadronic events.

(5) Each charged track (assumed to be a pion) and neutral track in the hemisphere is boosted into the rest frame of a τ moving along the thrust axis of the event with the beam energy in the laboratory frame. The magnitude of the vector sum of the particle momenta in this frame, which we call p^*, is a measure of the momentum carried by the neutrino in real τ decays assuming no initial- or final-state radiation. Events are accepted if p^* is less than 750 MeV/c. For $\tau^- \to \nu_\tau \pi^- \pi^+ \pi^- (\pi^0)$, Monte Carlo simulations show that in about 84% of the decays p^* is less than 750 MeV/c. In the data only about 14% of hadronic jets containing three charged particles have p^* less than 750 MeV/c. Jets produced via the two-photon interaction are also very unlikely to satisfy this condition.

The major decay modes of the τ which have the above properties are $\tau^- \to \nu_\tau \pi^- \pi^+ \pi^-$ and $\tau^- \to \nu_\tau \pi^- \pi^+ \pi^- \pi^0$ for which the previously measured branching fractions are about 8 and 5 %, respectively. They contribute approximately 60 and 40 %, respectively, to the tag assuming the above branching fractions.

As in the case of the one-prong tag, a cut is made on the charged-particle multiplicity and the invariant mass of the charged and neutral particles (assumed to be pions and photons, respectively) in the τ-decay candidate opposite the tag. Candidates with more than three charged particles or with mass greater than 2.5 GeV/c^2 are rejected. The number of τ candidates which pass all of the criteria for the three-prong tag is 1475.

IV. UNFOLDING THE BRANCHING FRACTIONS

A. Observed topologies

To determine the branching fractions, the tagged τ decays in each sample are divided into subgroups by charged- and neutral-particle multiplicity, and particle type where possible. The categories are chosen so that for each decay mode there is a category for which that decay mode is the major contributor with little contribution from other decay modes. Also, the criteria for the categories are chosen to be those that are well modeled by the Monte Carlo simulation program so that the systematic errors are kept to a minimum. The particle-identification algorithms used to unfold the branching fractions are *not* the same as those used to reject electrons and muons from the one-prong tag.

First, the tagged τ decays are divided into subgroups according to the number of charged particles in the hemisphere. If there is one charged particle, the decay is further classified according to the identification of that particle. Muons are defined to be tracks with momenta greater

than 2 GeV/c which penetrate all four layers of hadron absorber and have a signal within a search region equal to three times the root-mean-squared scattering distance in all four layers of proportional tubes. Electrons are identified from an algorithm[5] based on measurements of the ratio $r_i \equiv E_i/p$, where E_i is the energy deposition in the neighborhood of the track in one of four groupings, $i=1,2,3,4$, of readout layers in the LA calorimeter. The first three groupings combine all layers in the first 8 radiation lengths which have the same strip orientation; the fourth grouping combines the first three groupings. The algorithm demands that *each* value of r_i be greater than an appropriate minimum value $r_i^{\min}$. A track must have momentum greater than 1 GeV/c to be identified as an electron.

A track is defined to be a pion if it is *not* a muon and *not* an electron according to the muon and electron identification algorithms just described. Therefore, pion identification is only possible for tracks which project into the fiducial volume of the muon system *and* the LA calorimeter and which have momenta greater than 2 GeV/c. No kaon identification is used in this analysis.

Each decay candidate which has only one charged track is assigned to one of the following seven categories according to the direction and momentum of the track and its interaction with the muon system or LA calorimeters: (1) electron (e), (2) muon (μ), (3) pion (π), (4) not an electron ($\bar{e}$), (5) not a muon ($\bar{\mu}$), (6) no particle identification because of insufficient track momentum (x_p), (7) no particle identification because of track direction (x_d).

The details of the criteria for each of the above seven classifications are given in Table I. For example, consider a track with momentum greater than 2 GeV/c which projects into the muon system but leaves hits in less than four layers of the system, and which does not project into the LA calorimeter. There is sufficient information to reject the track as a muon but insufficient information to classify it as an electron or a pion. Therefore, the track is classified as not being a muon ($\bar{\mu}$).

To separate different modes involving one charged hadron, the tagged τ decays are further classified according to the number of neutral energy clusters in the hemisphere. First, it is necessary to apply a minimum energy cutoff for photons to reduce the number of spurious photons found due to hadronic interactions in the calorimeter and accidental overlap of energy in different layers of the calorimeter. For the sample corresponding to the one-prong tag, photons are defined to be neutral energy clusters with at least 650 MeV of energy. The candidates corresponding to the three-prong tag are less well contained within the LA system than the candidates for the one-prong tag because of the different geometrical acceptance for the two tags. Hence, the probability of detecting a photon in the three-prong-tag sample is lower. To increase the number of photons detected, the minimum energy cutoff is reduced to 500 MeV for the three-prong-tag sample at the expense of increasing the number of spurious photons. These cutoffs are varied to estimate the sensitivity of the measurements to spurious photons.

Candidates in category 3 (a pion), category 4 (not an electron), and category 5 (not a muon) are moved into categories 8, 9, 10, 11, and 12 if there are one, two, three, four, or more than four neutrals in the hemisphere, respectively (see Table II). Candidates in category 1 (an electron) and category 2 (a muon) with one or more neutrals in the hemisphere are moved into categories 13 and 14, respectively. These are usually due to hadronic decays in which a hadron passes the electron criteria, or a hadron decays to a muon or punches through the iron absorber simulating a muon. They can also be due to radiative leptonic decays.

To separate modes involving three charged particles, the tagged τ decays with two or three charged particles are separated into two categories according to whether or not there are any neutral energy clusters in the hemisphere. All of the topologies are shown in Table II along with the number of τ decays in each for the τ-candidate samples corresponding to the one-prong tag and the three-prong tag.

B. The unfold technique

From a Monte Carlo simulation, an efficiency matrix ϵ is determined whose elements ϵ_{ij} correspond to the probability of detecting a τ which decayed via mode j in the ith topology category. Let the number of events observed with topology i be N_i. The procedure is to find the set of branching fractions B_j which results in an "expected" distribution M_i, calculated from the efficiency matrix ϵ_{ij}, which maximizes the logarithm of the Poisson likelihood $\sum_i N_i \ln M_i$.

The minimization program MINUIT[6] is used to find the set of branching fractions which maximizes the logarithm likelihood. The program is also used to estimate the er-

TABLE I. Criteria for classification of a single charged particle.

Class	Momentum range (GeV/c)	In muon system fiducial volume	In LA fiducial volume	Criteria
e	$p>1$		Yes	$r_i \geq r_i^{\min}$
μ	$p>2$	Yes		4 muon layers hit
π	$p>2$	Yes	Yes	$r_i < r_i^{\min}$
$\bar{e}$	$1<p\leq 2$		Yes	$r_i < r_i^{\min}$
	$p>2$	No	Yes	$r_i < r_i^{\min}$
$\bar{\mu}$	$p>2$	Yes	No	<4 muon layers hit
x_p	$p\leq 1$			
	$1<p\leq 2$		No	
x_d	$p>2$	No	No	

TABLE II. The topological distribution of the raw τ-candidate samples corresponding to the one-prong tag and the three-prong tag. For each tag, the first column corresponds to the raw data sample, the second column corresponds to the background subtracted sample, and the third column corresponds to the best-fit distribution.

			One-prong tag			Three-prong tag		
Category	Particle identification	No. of photons	Raw sample	Background subtracted	Best fit	Raw sample	Background subtracted	Best fit
1	e	0	261	242	243	219	213	211
2	μ	0	170	166	159	109	109	103
3	π	0	169	167	164	78	73	73
4	$\bar{e}$	0	120	116	126	189	187	190
5	$\bar{\mu}$	0	30	28	23	19	19	15
6	x_p		128	127	128	166	164	166
7	x_d		20	19	25	92	89	101
8	π, $\bar{e}$, or $\bar{\mu}$	1	245	236	242	182	177	163
9	π, $\bar{e}$, or $\bar{\mu}$	2	141	135	124	96	93	105
10	π, $\bar{e}$, or $\bar{\mu}$	3	42	37		49	47	
11	π, $\bar{e}$, or $\bar{\mu}$	4	12	6	48	8	7	50
12	π, $\bar{e}$, or $\bar{\mu}$	>4	0	0		1	1	
13	e	>0	27	23	21	16	16	18
14	μ	>0	7	7	6	6	6	6
15	2 or 3 charged particles	0	120	110	110	102	98	98
16	2 or 3 charged particles	>0	135	111	111	143	136	136
	Total number of events		1627	1530	1530	1475	1435	1435

rors on the branching fractions by the standard technique of associating a change in the logarithm likelihood with confidence levels for a normal distribution.

C. Monte Carlo simulation

The Monte Carlo simulation is based on an event generator for $e^+e^-\to\tau^+\tau^-(\gamma)$ written by Berends and Kleiss[7] which includes the emission of real photons from the initial- and final-state leptons, virtual radiative corrections to the lepton-photon vertex, multiple photon exchange, and vacuum-polarization corrections. The generated τ's decay according to branching fractions close to the measured branching fractions. This analysis is not sensitive to the specific branching fractions used in the Monte Carlo simulation. The following decay modes are included: $\tau^-\to\nu_\tau e^-\bar{\nu}_e$, $\tau^-\to\nu_\tau\mu^-\bar{\nu}_\mu$, $\tau^-\to\nu_\tau\pi^-$, $\tau^-\to\nu_\tau\rho^-$, $\tau^-\to\nu_\tau A_1^-$, $\tau^-\to\nu_\tau(4\pi)^-$, $\tau^-\to\nu_\tau K^-$, and $\tau^-\to\nu_\tau K^{*-}$. Breit-Wigner mass distributions with the known masses and widths are used for the ρ, K^*, and A_1. The mass of the 4π mode is distributed according to isotropic phase space in the τ center of mass frame. The vector mesons ρ and K^{*-} are produced only in the two allowed helicity states.

All particles are propagated through the detector, decaying according to the known lifetimes and branching fractions. Multiple scattering, bremsstrahlung, and photon conversions are simulated. The simulation of electromagnetic interactions in the LA system is based on the EGS shower code.[8] The simulation of hadronic interactions in the LA system is based on a library of real pion interactions recorded in a pion-beam test.

D. Particle-identification efficiency

Tracks corresponding to particles of known identity in the data are used to determine the particle-identification efficiencies for the unfold matrix. The efficiency for lepton identification is estimated from two sources of known leptons in the data: single-photon production of e^+e^- and $\mu^+\mu^-$ pairs, and two-photon production of e^+e^- and $\mu^+\mu^-$ pairs. Together these samples cover most of the relevant momentum range. The selection criteria for these events are described in Appendix B. The three tracks in the three-prong tag are used to determine pion identification efficiencies.

Muon identification. The probability that a muon has associated hits in all four layers of the muon system, if the track trajectory projects into the fiducial volume of the muon system, is estimated from an unbiased sample of muons from single- and two-photon production of muon pairs. The muon identification efficiency is found to vary from 88% at 2 GeV/c to 92% at 14 GeV/c. The identification efficiency is also studied as a function of the polar angle of the track. Since low-momentum tracks scatter through larger angles than high-momentum tracks when passing through material, a muon with low momentum near the edge of the module is more likely to scatter out of the module and fail the criteria for a muon. The efficiency is lower near the edge of the module for low-momentum tracks while there is little dependence of the efficiency on the polar angle for high-momentum tracks. This dependence on polar angle is seen in both the Monte Carlo simulation and the data. Of course, the efficiency also depends slightly on the azimuthal angle for the same

reason.

Electron identification. The probability that an electron passes the electron identification criteria is estimated from an unbiased sample of electrons from single- and two-photon production of electron pairs. For the sample of known electrons from radiative Bhabha events, the electron candidate is used only if the photon is in a different LA module. The electron identification efficiency is found to vary from 93% at 1 GeV/c to 96% at 14 GeV/c. No significant dependence of the efficiency on polar angle is seen in the data or in the Monte Carlo simulation.

Pion identification. For the purpose of this analysis, a pion is defined to be a track which meets the momentum and fiducial-volume criteria for μ/π and e/π discrimination and does not satisfy the requirements to be identified as a muon or an electron. The probability that a pion which meets the momentum and fiducial volume criteria for muon identification has associated hits in all four levels of the muon system is determined with pions from three-prong decays of the τ. This probability is measured to be $(1.4\pm0.4)\%$ in the data. It is estimated that about half of the pions in the data which pass the criteria for a muon are due to the decay of the π to $\mu\nu_\mu$ in flight, and about half are due to hadronic punchthrough and track overlap. The probability of misidentifying a single prong hadron as a muon is actually slightly lower than this because there is no overlap of hits from other tracks. However, the difference has a negligible effect on the measured branching fractions.

The probability that a pion which meets the momentum and fiducial volume criteria for electron identification fails the electron identification criteria is found to be about $(96.5\pm1.5)\%$ for pions from three-prong decays of the τ. This probability is slightly higher for isolated pions. The efficiency for e/π discrimination also depends on the number of photons and other charged tracks in the vicinity of the track. For example, the pion identification efficiency is about 1.5% higher for pions which are from a three-prong decay of the τ with no detected neutrals than for those with a detected neutral, in both the data and the Monte Carlo simulation.

Most decay modes with one charged hadron in the final state also have at least one neutral pion in the final state. Therefore, if the hadron is misidentified as an electron, the decay is usually classified as an electron accompanied by at least one detected neutral. This does not mix with the electron decay mode unless radiative decays are important.

Photon identification. Photons are identified with an algorithm which searches for clusters of energy in the LA calorimeter not associated with a charged track. Spurious photon candidates which are not due to real photons can result from the coincidence of noise fluctuations and real deposited energy, or from hadronic interactions in the LA calorimeter which deposit energy far from the charged track. In an independent analysis,[9] it was found that the probability of finding a spurious photon in a three-prong τ decay is about $(50\pm25)\%$ higher in the data than in the Monte Carlo simulation with a minimum energy cutoff of about 600—800 MeV. The appropriate elements in the efficiency matrix are adjusted accordingly for both the single-prong and multiprong decays.

E. Angular distribution

The angular distribution of the τ candidates in the sample affects the particle-identification efficiencies because of the limited active volume of each detector component. The decay products from the two τ's are quite collinear because of the large boost due to the high momentum of each τ in the laboratory frame. Therefore, the direction of the decay products in the τ sample is correlated with the direction of the decay products in the tag. Consequently, agreement between the angular distribution of the tag in the data and the Monte Carlo simulation provides a check on the accuracy of the angular-dependent part of the Monte Carlo—generated efficiency matrix.

The angular distribution of the single charged track in the one-prong tag is shown in Fig. 2 for the data and the τ Monte Carlo simulation. Figure 2(a) shows the $|\cos\theta|$ distribution where θ is the polar angle relative to the beam; Fig. 2(b) shows the azimuthal angle ϕ between the track and the horizontal plane. For lepton rejection, the charged track in the one-prong tag must project into the active volumes of the muon system and the LA calorimeter. The large gaps in ϕ, 45° from the horizontal plane, correspond to gaps between the four walls of the muon

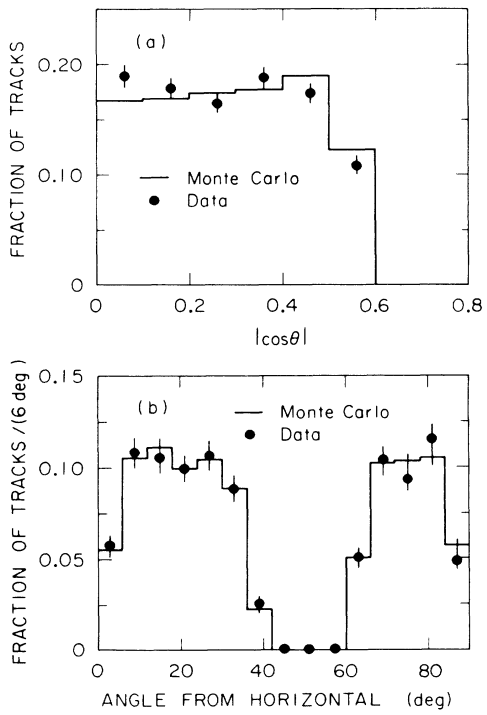

FIG. 2. Angular distribution of the single charged track in the one-prong tag. The histogram corresponds to the Monte Carlo simulation and the symbol ● corresponds to the data. (a) shows the distribution of tracks as a function of $|\cos\theta|$ where θ is the polar angle of the track relative to the beam. (b) shows the distribution of tracks as a function of the azimuthal angle relative to the horizontal plane.

system. The smaller gaps in ϕ, at 0° and 90° from the horizontal plane, correspond to the gaps between the eight LA modules. The agreement between the Monte Carlo simulation and the data is good.

The distribution of the polar angle for the three charged tracks in the three-prong tag is shown in Fig. 3 for the data and the τ Monte Carlo simulation. The agreement is quite good. Since there is no electron or muon identification criteria applied to the three-prong tag, the distribution of tracks is flat in ϕ.

F. Momentum distribution

The momentum distributions of the tagged particles affects the particle-identification efficiency because of the minimum-momentum cutoff of 1 GeV/c for electron identification and 2 GeV/c for muon identification. The momentum distributions of all single charged particles in the τ-candidate samples are shown in Figs. 4(a) and 4(b) for the one-prong tag and the three-prong tag, respectively. The distributions are shown for both the data and the Monte Carlo simulation. The branching fractions affect the distributions since the momentum spectrum is different for each decay mode. The branching fractions used in the Monte Carlo simulation are close to those measured with the data. The fact that the agreement is quite good indicates that the background contributions to the samples are not large.

G. The efficiency matrix

The efficiency matrix for each tag is determined from a combination of Monte Carlo simulation and particle-identification efficiencies determined from the data as described above. Table III shows the efficiency matrix for the one-prong tag. The first column lists the decay modes and the second column lists the relative efficiency for each decay mode to be included in the final sample of τ-decay candidates corresponding to the one-prong tag. The errors on the relative efficiencies are statistical errors only. The Monte Carlo sample is equivalent to four times the data sample. These relative efficiencies reflect any biases introduced by the selection criteria. Any uncertainty in the bias results in an equal fractional uncertainty in the branching fractions. The absolute efficiency does not enter into this analysis since the branching fractions are constrained to add up to unity. The remaining columns list the probability (in percent) for each decay mode to be classified into each of the above categories, given that the decay has been tagged.

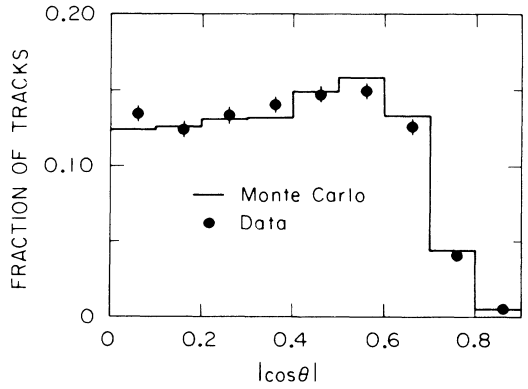

FIG. 3. Angular distribution of the three charged tracks in the three-prong tag. The histogram corresponds to the Monte Carlo simulation and the symbol ● corresponds to the data.

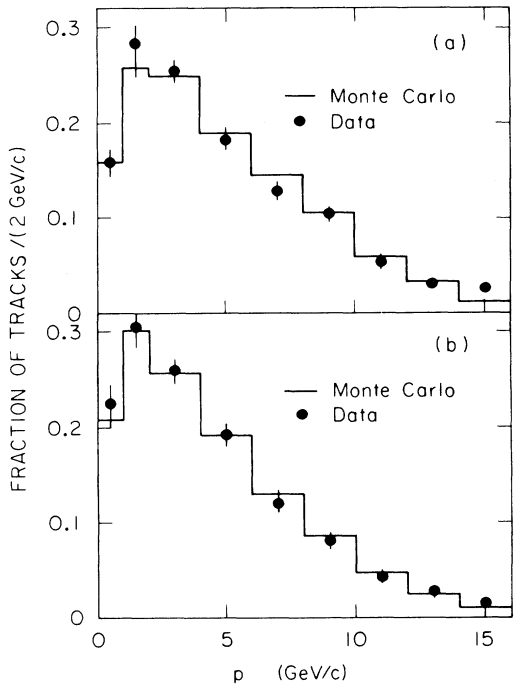

FIG. 4. Momentum distributions of single charged particles in the τ-candidate samples corresponding to the one-prong tag (a) and the three-prong tag (b). The histogram corresponds to the Monte Carlo simulation and the symbol ● corresponds to the data.

The efficiency matrix for the three-prong tag is shown in Table IV. This matrix is less diagonal than that for the one-prong tag. For example, if a τ decays via the mode $\tau^- \rightarrow \nu_\tau \mu^- \bar{\nu}_\mu$ and is tagged, the probability that it is classified as a muon (category 2) is about 58% for the one-prong tag and about 34% for the three-prong tag. This difference is due to the different fiducial volume criteria for the two tags. For the one-prong tag, the single charged particle in the hemisphere must pass through the active volume of both the LA calorimeter and the muon system. Since the decay products of the two τ's in the pair are quite collinear, τ-decay candidates opposite the one-prong tag are likely to also pass through the active parts of the detector. The geometrical criteria for the three-prong tag are much looser.

V. BACKGROUNDS

The potential sources of background are single-photon production of e^+e^- and $\mu^+\mu^-$ pairs, two-photon production of e^+e^-, $\mu^+\mu^-$, $\tau^+\tau^-$, and $q\bar{q}$ pairs, and single-photon production of $q\bar{q}$ pairs leading to hadronic jets.

TABLE III. Monte Carlo–generated efficiency matrix for the one-prong tag. The efficiencies in the third through last columns are expressed in percent.

Decay mode $\tau^- \to$	Relative total efficiency	1 charged particle: 0γ e	0γ μ	0γ π	0γ $\bar{e}$	0γ $\bar{\mu}$	1γ	2γ	3γ	4γ	$>4\gamma$	$>0\gamma$ e	$>0\gamma$ μ	Any number of γ's x_p	Any number of γ's x_d	2 or 3 prong 0γ	2 or 3 prong $>0\gamma$
							π, $\bar{e}$, or $\bar{\mu}$										
$e^-\bar{\nu}_e\nu_\tau$	1.00±0.02	80.1		2.2	1.3	4.2	0.7					0.1		9.1	2.0	0.3	
$\mu^-\bar{\nu}_\mu\nu_\tau$	1.04±0.02		57.5	5.2	26.3	0.3	0.1						0.2	8.2	2.1	0.1	
$\pi^-\nu_\tau$	0.97±0.03	2.1	1.0	57.4	17.9	3.8	10.1	1.4						4.3	1.8		0.2
$\pi^-\pi^0\nu_\tau$	1.02±0.02	0.9		8.3	3.8	0.6	45.4	17.4	1.6	0.2		2.5	1.0	11.0	1.9	2.3	3.1
$\pi^-2\pi^0\nu_\tau$	0.99±0.04	0.7		2.2	1.2		22.1	26.2	13.1	2.5	0.3	4.5	1.0	13.0	1.5	1.3	10.4
$\pi^-3\pi^0\nu_\tau$	0.92±0.05				1.3		7.6	18.1	20.5	11.4	1.6	8.5	1.0	13.1	0.5	1.4	15.0
$\pi^-\pi^+\pi^-\nu_\tau$	1.06±0.04			0.6		0.2	0.4	0.2								72.3	26.3
$\pi^-\pi^+\pi^-\pi^0\nu_\tau$	1.00±0.05		0.3				0.3	1.0						0.3		22.7	75.4
$K^-\nu_\tau$	0.95±0.14			66.7	22.2	8.3								2.8			
$K^{*-}\nu_\tau$	0.98±0.10	1.3	1.3	21.1	5.3	2.6	17.1	9.3	2.6					9.2	3.9	23.7	2.6

TABLE IV. Monte Carlo–generated efficiency matrix for the three-prong tag. The efficiencies in the third through last columns are expressed in percent.

Decay mode $\tau^- \to$	Relative total efficiency	1 charged particle: 0γ e	0γ μ	0γ π	0γ $\bar{e}$	0γ $\bar{\mu}$	1γ	2γ	3γ	4γ	$>4\gamma$	$>0\gamma$ e	$>0\gamma$ μ	Any number of γ's x_p	Any number of γ's x_d	2 or 3 prong 0γ	2 or 3 prong $>0\gamma$
							π, $\bar{e}$, or $\bar{\mu}$										
$e^-\bar{\nu}_e\nu_\tau$	1.00±0.02	71.1		1.5	2.1	2.7	0.2					0.4		13.4	8.5	0.1	
$\mu^-\bar{\nu}_\mu\nu_\tau$	1.03±0.02		33.6	3.4	40.5	0.2	0.2						0.2	12.4	9.4	0.1	
$\pi^-\nu_\tau$	0.94±0.03	2.8	1.0	33.6	32.0	4.2	6.9	1.0				0.1		9.6	8.8		
$\pi^-\pi^0\nu_\tau$	0.91±0.02	0.5		4.0	5.0	0.5	36.7	19.4	2.8	0.1		2.7	1.0	15.7	7.3	2.1	2.2
$\pi^-2\pi^0\nu_\tau$	0.91±0.04	0.3		0.5	1.0	0.2	12.5	23.6	18.8	5.2	0.9	4.6	1.0	14.0	7.4	1.2	8.8
$\pi^-3\pi^0\nu_\tau$	0.86±0.05	0.7		0.7	1.0		6.3	12.2	18.7	10.9	4.4	6.3	1.0	17.3	4.9		15.6
$\pi^-\pi^+\pi^-\nu_\tau$	0.87±0.04	0.7	0.5	0.2	1.2		1.0					0.2		0.5	0.2	69.4	26.1
$\pi^-\pi^+\pi^-\pi^0\nu_\tau$	0.91±0.05	0.8		0.3	0.6		0.8	0.5	0.3		0.3			0.8	0.3	15.1	80.2
$K^-\nu_\tau$	0.92±0.14	7.7		46.2	28.9	3.8								1.9	11.5		
$K^{*-}\nu_\tau$	0.97±0.10	1.9		15.2	19.1		15.2	16.2						5.7	4.8	20.0	1.9

TABLE V. Estimated background in the one-prong and three-prong tag samples.

Source $e^+e^- \rightarrow$	Number of background events One-prong tag	Three-prong tag
$e^+e^-(\gamma)$	4.5±0.9	4
$\mu^+\mu^-(\gamma)$	0.5±0.2	0
$e^+e^-e^+e^-$	4.7±0.9	0
$e^+e^-\mu^+\mu^-$	4.4±1.6	0
$e^+e^-\tau^+\tau^-$	35±5	15±3
$e^+e^-q\bar{q}$	0	0
$q\bar{q}$	52±16	20±4

The estimated background from each source is discussed below and summarized in Table V. The discussion of backgrounds from two-photon production of τ pairs and $q\bar{q}$ pairs is combined for both samples in the same section. Then the other sources of background are discussed for the two tags separately since they contribute to them in quite different ways.

A. Background from two-photon production of τ pairs

A sample of Monte Carlo–simulated events of two-photon production of τ pairs, equivalent to an integrated luminosity of about 270 pb^{-1}, is subjected to all of the selection criteria for each tag. The number of charged particles which pass the cuts is used to predict the total background in the τ-candidate sample. The background contribution from $e^+e^- \rightarrow e^+e^-\tau^+\tau^-$, expected in 207 pb^{-1}, is (35±5) events for the one-prong tag and (15±3) for the three-prong tag. This background constitutes (2.1±0.3)% and (1.0±0.2)% of the signal for the samples corresponding to the one-prong tag and the three-prong tag, respectively. The Monte Carlo simulation is used to determine the contribution of this background to each category separately.

About a third of the τ candidates in the Monte Carlo background sample corresponding to the one-prong tag are classified as electrons. The remainder are scattered among the other categories. The fraction identified as electrons is significantly larger than the fraction identified as muons or pions for several reasons. First of all, an event with total energy less than $E_{\text{beam}}/2$ is not accepted unless it contains an electron with $p > 1.25$ GeV/c, or a track with associated hits in three of the four muon chamber levels. Since the LA calorimeters cover a larger solid angle than the muon system, an event with an electron in it is more likely to pass than an event with a muon in it. Second, the momentum spectrum of the charged particles is peaked at the low end, and the minimum momentum required for muon or pion identification is 2 GeV/c, while that for electron identification is only 1 GeV/c. This background constitutes (4.4±1.2)% of the electron signal in the sample corresponding to the one-prong tag.

B. Background from two-photon production of $q\bar{q}$

The overall event criteria $E_{\text{ch}} > E_{\text{beam}}/4$ and $E_{\text{tot}} > E_{\text{beam}}/2$ if none of the tracks in the event is identified as an electron or a muon (see Sec. III) eliminate most background from two-photon production of $q\bar{q}$ pairs. In addition, the cut on p^* for the three-prong tag, and the requirement of a track with at least 2 GeV/c momentum at $|\cos\theta|$ less than about 0.6 for the one-prong tag, provide rejection against this background.

C. Backgrounds to the one-prong tag

Leptonic backgrounds. The background due to electrons and muons satisfying the lepton rejection criteria for the single charged particle in the one-prong tag is estimated as follows. All of the criteria for the one-prong tag, *except* the lepton rejection cuts, are applied to Monte Carlo simulations of single- and two-photon production of lepton pairs. This results in a large number of events passing the momentum cuts and fiducial volume requirements of the one-prong tag. Then the measured efficiency for lepton rejection is used to estimate the background from these sources.

The muon rejection efficiency is measured from an unbiased sample of 4923 muon candidates from the data (see Appendix B) which pass the fiducial volume criteria for muon rejection. The measured muon rejection inefficiency is (0.14±0.05)%. The electron rejection efficiency is measured from an unbiased sample of 15 555 electron candidates from the data (see Appendix B) with momentum greater than 1 GeV/c and less than 14 GeV/c, projecting into the active volume of the LA calorimeter. The measured electron rejection inefficiency is (0.15±0.03)%.

The measured muon and electron rejection inefficiencies plus the Monte Carlo simulations lead to the estimated backgrounds shown in Table V for single- and two-photon production of lepton pairs. The distribution of the background among the various topologies is also determined from the Monte Carlo simulation. For single-photon production of lepton pairs, most of the events which pass the selection criteria correspond to the production of a photon and two leptons with approximately equal energy in which the photon travels down the beam pipe and is undetected.

Background from single-photon production of $q\bar{q}$. The background in the τ-candidate sample from hadronic events is estimated from the invariant-mass distribution of the candidate τ decays before the cut on invariant mass. The background is calculated separately for the sample of candidates with one charged particle and more than one charged particle. The procedure is outlined here for the candidates with more than one charged particle. The invariant mass of the charged particles and neutrals particles is calculated for each candidate τ decay. In the sample before the cut on invariant mass, (14±2)% of the candidates have an invariant mass greater than 2.5 GeV/c^2. For a similar sample of τ decays in the Monte Carlo simulation, only (2.8±0.7)% have mass greater than 2.5 GeV/c^2. Also, a sample of hadronic events with three charged particles in one hemisphere and at least six charged particles in the other hemisphere is selected from the data and used to determine that (55±2)% of hadronic three-prong jets have mass greater than 2.5 GeV/c^2. These numbers are used to estimate that 28±6 of the 255

two- and three-prong τ candidates with mass less than 2.5 GeV/c^2 are due to hadronic background. In the sample of hadronic three prongs (with mass less than 2.5 GeV/c^2) from the data, (74±2)% have at least one neutral particle in the three-prong jet. This is used to determine the distribution of the background between the topologies with zero or greater than zero neutral particles.

A similar analysis applied to the candidates with one charged particle leads to an estimate of 24±10 hadronic background events among the 1372 candidates. A hadronic sample with one charged particle in one hemisphere and at least six in the other hemisphere is used to determine the distribution of the background events among the topologies with various neutral multiplicities.

D. Background to the three-prong tag

Background from single- or two-photon production of lepton pairs. The potential sources of background to the three-prong tag are single- and two-photon production of lepton pairs with initial- or final-state radiation in which the radiated photon converts to an e^+e^- pair. Among these, the dominant potential source is radiative Bhabha events because of the large cross section for this process. The criteria which eliminate this background are the rejection of events in which the total energy (charged plus neutral) in the three-prong tag is greater than 14 GeV or in which an oppositely charged pair of tracks in the three-prong tag has a small opening angle. The pair-finding algorithm is very efficient for radiative Bhabha events for the following reasons. First, since the event has three tracks in one hemisphere, asymmetric conversions in which one of the charged particles from the pair is not detected will not contribute to the background. Also, since the photon is typically emitted at a very small angle to the electron, the opening angle between the members of the pair and the primary electron will also be small. Therefore, even if one member of the pair is not well tracked, the other member of the pair and the primary electron are likely to satisfy the criteria for a pair if they are oppositely charged. Finally, because of the low multiplicity of the event, the tracking quality is quite good and hence the pair-finding efficiency is high.

From Monte Carlo–generated events, the estimated background due to lepton pairs with a photon conversion is negligible. A hand scan of all events in the data with the τ candidate opposite the three-prong tag identified as an electron, muon, or pion reveals four, zero, and one event from these sources for the electron, muon, and pion topologies, respectively.

Background from single-photon production of q-$\bar{q}$. A sample of hadronic events with three charged particles in one hemisphere and at least six charged particles in the other hemisphere is selected from the data using all of the selection criteria for the three-prong tag except the cuts on p^* and the invariant mass of the three-prong side. From this sample, it is determined that (14.2±1.6)% of three-prong hadronic jets pass the p^* cut ($p^* \leq 750$ MeV/c), and, of these, (52±6)% pass the mass cut ($m_3 < 1.7$ GeV/c^2). From a Monte Carlo simulation of τ-pair production, it is determined that (84±1)% of τ's decaying to three charged particles pass the p^* cut.

The sample of τ candidates tagged with the three-prong tag contains 567 decays with two or three charged particles before the p^* and invariant-mass cuts have been applied to the three-prong tag, and 265 events after the p^* cut. Using the known fraction of hadronic jets and τ decays which survive the p^* cut, one can calculate that the sample of 265 decays contains 43±6 hadronic jets. Since the invariant-mass cut on the three-prong tag removes a further (48±6)% of the hadronic events, the hadronic background in the two and three prong sample, after the p^* and mass cuts on the three-prong tag, is 22±4 events. After this, a cut of 2.5 GeV/c^2 is made on the invariant mass of the τ candidates opposite the three-prong tag. This also eliminates some of the hadronic background, leaving a background of 10±3 events or (4±2)% of the total two- and three-prong sample.

A similar analysis applied to the sample of one-prong τ candidates tagged with the three-prong tag leads to an estimated hadronic background of 10±2 events or (0.8±0.2)% of the one prong sample.

The distribution of the hadronic background among topologies with different number of neutrals is determined from the sample of hadronic events with a one- or three-prong jet versus a six-prong jet in the data.

VI. RESULTS

A. Measured branching fractions

The background subtracted distributions of τ-decay candidates corresponding to the one-prong tag and the three-prong tag are shown in the second column for each tag in Table II. A maximum-likelihood fit is used to estimate the branching fractions from these background subtracted distributions. Because of the large uncertainties in the photon-identification efficiency, and the amount of mixing of decay modes with two or more neutral pions in the final state among topologies with three or more detected photons, it is very difficult to determine branching fractions for $\tau^- \to \nu_\tau \pi^- 2\pi^0$ and $\tau^- \to \nu_\tau \pi^- 3\pi^0$ separately, using this method. The results depend heavily on the minimum energy cutoff for a neutral energy cluster and the probability of finding spurious photons. Consequently, the three categories with a charged pion (π, $\bar{e}$, or $\bar{\mu}$) and three, four, or more than four photons are combined into one category for the fit. Also, the decay modes $\tau^- \to \nu_\tau \pi^- 2\pi^0$ and $\tau^- \to \nu_\tau \pi^- 3\pi^0$ are combined assuming a nominal value of four for the ratio of $B(\tau^- \to \nu_\tau \pi^- 2\pi^0)$ to $B(\tau^- \to \nu_\tau \pi^- 3\pi^0)$ to calculate the corresponding row in the efficiency matrix. This ratio is varied to estimate the systematic errors due to the uncertainty in the ratio.

Since no K/π separation is attempted in this analysis, the branching fractions for $\tau^- \to \nu_\tau K^-$ and $\tau^- \to \nu_\tau K^{*-}$ are fixed at the measured values of (0.6±0.2)% by DELCO[10] for $\tau^- \to \nu_\tau K^-$ and (1.3±0.4)% by Mark II (Ref. 11) for $\tau^- \to \nu_\tau K^{*-}$.

The distribution corresponding to the branching fractions which result in a maximum of the likelihood function are shown in the third column of Table II for the samples corresponding to each tag. The measured branching fractions are shown in Table VI. The first er-

ror listed for each measurement corresponds to a half unit change in the log likelihood.

B. Systematic errors

Systematic errors are introduced by uncertainties in particle-identification efficiencies, relative overall efficiencies for each decay mode, and background estimates. The size of the uncertainties are discussed in the following sections and the resulting systematic errors are summarized in Table VII.

Particle-identification efficiency

The uncertainty in the electron-identification efficiency, estimated to be 3%, is small because of the large, clean, unbiased sample of electrons available in the data for checking the efficiency. The uncertainty in pion-identification efficiency, estimated to be 4%, is slightly higher since clean samples of isolated charged pions, with a known number of neutral pions accompanying them, are difficult to find in the data. Variations in the branching fractions are estimated for changes in the electron- and pion-identification efficiencies equal to the uncertainty.

In addition, the analysis is repeated using different cutoff values of $r_i^{\min}$ for e/π discrimination where a low cutoff value results in a clean pion sample, and a high cutoff value results in a clean electron sample. The dependence of the results on the cutoff value of $r_i^{\min}$ used in the analysis is negligible.

The uncertainty in the muon-identification efficiency, estimated to be 3%, is small because of the clean sample of muons available for checking the efficiency. The uncertainty in the probability for a pion to pass the identification criteria for a muon is estimated to be 30%. The effect of this uncertainty on the results is negligible.

As described in Sec. IV, the number of spurious photons in the data is estimated to be higher than the number predicted by the Monte Carlo simulation by (50±25)%. The number of spurious photons is varied within this estimate to determine the dependence of the branching fractions on photon identification. The sensitivity to photon identification is also estimated by varying the cutoff used for the minimum energy of a neutral energy cluster. The results for $B(\tau^- \to \nu_\tau \pi^- \pi^0)$ and $B(\tau^- \to \nu_\tau \pi^+ (2 \text{ or } 3\pi^0))$ are the most sensitive to this cutoff since a low cutoff increases the number of spurious photons found, while a high cutoff eliminates real photons, both effects resulting in a loss of discriminating power for these two modes. This sensitivity is included in the systematic error due to photon identification.

The decay modes $\tau^- \to \nu_\tau \pi^- 2\pi^0$ and $\tau^- \to \nu_\tau \pi^- 3\pi^0$ are combined assuming a nominal value of four for the ratio of $B(\tau^- \to \nu_\tau \pi^- 2\pi^0)$ to $B(\tau^- \to \nu_\tau \pi^- 3\pi^0)$ to calculate the corresponding row in the efficiency matrix. The value of this ratio is varied between two and eight to estimate the systematic errors due to the uncertainty in the ratio. The errors introduced due to the uncertainty in this ratio are small compared to other systematic errors.

Relative overall efficiency. The uncertainty in the branching fractions due to the bias in the sample is directly proportional to the uncertainty in the relative overall efficiency for each decay mode. These relative efficiencies, determined from the Monte Carlo simulation, are listed in Tables III and IV for the one-prong tag and the three-prong tag, respectively. The errors listed in these tables are statistical errors only. Within each sample, there is little or no dependence of the relative efficiency on the decay mode of the tag, according to the Monte Carlo simulation. For example, in the one-prong-tag sample, the relative efficiencies do not depend on whether the tag corresponds to $\tau^- \to \nu_\tau \pi^-$ or $\tau^- \to \nu_\tau \rho^-$.

The Monte Carlo simulation does not predict any significant differences in efficiency for different decay modes for the sample corresponding to the one-prong tag. However, it does predict that the electron and muon decay modes are slightly more likely to be included in the sample corresponding to the three-prong tag. The uncertainty in the relative overall efficiency for each decay mode is estimated to contribute an absolute error of 0.8% to each branching fraction. For the electron and muon decay modes this corresponds to a relative error of about 4.5%.

Background estimates. The errors due to the uncertainty in the backgrounds are estimated by varying the backgrounds within the ranges shown in Table V. The background from each independent source is varied separately. The errors from the uncertainties in background are generally small compared to the overall systematic errors.

Summary of systematic errors. A summary of the abso-

TABLE VI. The measured branching fractions in percent. For each measurement, the first error is statistical and the second is systematic.

Decay mode $\tau^- \to$	One-prong tag	Three-prong tag	Average
$e^- \bar{\nu}_e \nu_\tau$	19.5±1.2±1.3	18.8±1.2±1.2	19.1±0.8±1.1
$\mu^- \bar{\nu}_\mu \nu_\tau$	17.6±1.2±1.0	19.2±1.4±1.0	18.3±0.9±0.8
$\pi^- \nu_\tau$	11.4±1.4±1.5	7.7±1.7±1.5	10.0±1.1±1.4
$\pi^- \pi^0 \nu_\tau$	25.3±2.6±2.7	26.3±2.3±2.5	25.8±1.7±2.5
$\pi^- (n\pi^0, n>1) \nu_\tau$	14.1±2.2±2.8	10.6±1.8±2.5	12.0±1.4±2.5
$\pi^- \pi^+ \pi^- \nu_\tau$	6.1±1.1±1.2	7.2±1.1±1.0	6.7±0.8±0.9
$\pi^- \pi^+ \pi^- (n\pi^0, n>0) \nu_\tau$	4.0±1.2±1.2	8.2±1.2±1.0	6.1±0.8±0.9
$K^- \nu_\tau$		Fixed at 0.7%	
$(K\pi)^- \nu_\tau$		Fixed at 1.3%	

TABLE VII. Absolute systematic errors (in percent) for the measurements corresponding to the one-prong tag and the three-prong tag.

Decay mode $\tau^- \rightarrow$	Source of error: Uncertainty in	One-prong tag Absolute error (%)	Three-prong tag Absolute error (%)
All modes	relative overall efficiencies	0.8	0.8
$e^-\bar{\nu}_e\nu_\tau$	e/π discrimination for $e^\pm$	0.6	0.6
	e/π discrimination for $\pi^\pm$	0.7	0.5
	backgrounds	0.4	0.3
	Total	1.3	1.2
$\mu^-\bar{\nu}_\mu\nu_\tau$	μ/π discrimination for $\mu^\pm$	0.5	0.5
	backgrounds	0.3	0.2
	Total	1.0	1.0
$\pi^-\nu_\tau$	e/π discrimination for $e^\pm$	0.5	0.6
	e/π discrimination for $\pi^\pm$	0.6	0.4
	μ/π discrimination for $\mu^\pm$	0.6	0.6
	photon identification	0.8	0.8
	backgrounds	0.2	0.2
	Total	1.5	1.5
$\pi^-\pi^0\nu_\tau$	e/π discrimination for $\pi^\pm$	1.2	1.1
	ratio of $B(\pi^-2\pi^0)$ to $B(\pi^-3\pi^0)$	1.0	0.4
	photon identification	2.0	2.0
	backgrounds	0.3	0.2
	Total	2.7	2.5
$\pi^-(2 \text{ or } 3\pi^0)\nu_\tau$	e/π discrimination for $\pi^\pm$	1.2	1.1
	ratio of $B(\pi^-2\pi^0)$ to $B(\pi^-3\pi^0)$	1.0	0.4
	photon identification	2.0	2.0
	backgrounds	0.8	0.2
	Total	2.8	2.5
$\pi^-(n\pi^0)\nu_\tau$	e/π discrimination for $\pi^\pm$	0.3	0.3
$n=1,2,3$	ratio of $B(\pi^-2\pi^0)$ to $B(\pi^-3\pi^0)$	0.1	0.2
(sum of above	photon identification	0.8	0.6
two modes)	backgrounds	1.0	0.4
	Total	1.5	1.1
$\pi^-\pi^+\pi^-\nu_\tau$	photon identification	0.6	0.6
	backgrounds	0.7	0.3
	Total	1.2	1.0
$\pi^-\pi^+\pi^-\pi^0\nu_\tau$	photon identification	0.6	0.6
	backgrounds	0.7	0.3
	Total	1.2	1.0

lute systematic errors for each branching fraction is shown in Table VII. The major contributions to the systematic errors for the leptonic decay modes are the uncertainties in the relative overall efficiencies and the particle-identification efficiencies. For the hadronic modes, the major contribution to the error is the uncertainty in photon identification. For all the decay modes, the total systematic error is approximately the same size as the statistical error from the maximum-likelihood fit.

Many of the systematic errors for different branching fractions are highly correlated. Therefore, the systematic error on the sum of the branching fractions for two decay modes must be calculated with the correlations taken into account. An example of this is shown in Table VII for the sum of the branching fractions for the decay modes $\tau^- \rightarrow \nu_\tau\pi^-\pi^0$ and $\tau^- \rightarrow \nu_\tau\pi^-(2 \text{ or } 3\pi^0)$. The systematic error on the sum of the two branching fractions is less than that on each branching fraction separately.

C. Discussion of results

The measured branching fractions for the τ-candidate samples corresponding to the one-prong tag and the three-prong tag are shown in Table VI. For each branching fraction, the first error is statistical and the second is systematic. The statistically weighted average of the measurements corresponding to the two tags is also shown for

each branching fraction. The systematic error for the weighted average is obtained by averaging systematic errors common to the two samples linearly (for example, particle-identification efficiency), and independent systematic errors quadratically (for example, backgrounds).

In the Monte Carlo simulation, the maximum number of π^0's accompanying a single charged pion and three charged pions is three and one, respectively. However, the categories for the fit are chosen so that decay modes involving more π^0's will be included in the measured branching fraction with the largest number of π^0's. The decay modes listed in Table VI reflect this fact.

In this analysis the sum of the branching fractions is constrained to one. Since the decay modes used in the fit are only those for which the branching fractions have been measured in other experiments, and since the sum of the previously measured branching fractions is less than one, this analysis must result in a larger branching fraction than the world average for at least one mode.

The following comments summarize the results.

(1) The total branching fraction to three charged pions is measured to be $(12.8\pm1.0\pm0.7)\%$ which is in good agreement with our recent measurement[12] of $(12.5\pm0.5\pm0.8)\%$ and with the world average of $(13.2\pm0.2)\%$. The ratio of $B(\tau^-\to\nu_\tau\pi^-\pi^+\pi^-)$ to $B(\tau^-\to\nu_\tau\pi^-\pi^+\pi^-\pi^0)$ is also in agreement with the world average.[13]

(2) For each tag, both leptonic branching fractions are found to be about one standard deviation higher than the world average.[13] The measured leptonic branching fractions correspond to a τ lifetime of $(3.0\pm0.2)\times10^{-13}$ s. The average measured τ lifetime[13] is $(2.8\pm0.2)\times10^{-13}$ s. Therefore, the leptonic branching fractions measured in this analysis are consistent with the measured τ lifetime.

(3) The theoretical prediction[1] for the ratio of $B(\tau^-\to\nu_\tau\pi^-)$ to $B(\tau^-\to\nu_\tau e^-\bar{\nu}_e)$ is 0.607. Combining this with the measured leptonic branching fractions from this analysis leads to a prediction of $B(\tau^-\to\nu_\tau\pi^-)=(11.4\pm0.6)\%$ which is $(1.4\pm1.9)\%$ higher than the measured value of $(10.0\pm1.1\pm1.4)\%$.

(4) The measurements of the branching fractions for the decay modes $\tau^-\to\nu_\tau\pi^-\pi^0$ and $\tau^-\to\nu_\tau\pi^-(2$ or $3\pi^0)$ have large errors which are highly correlated. The sum of these two measurements is $(37.8\pm1.2\pm1.0)\%$ where the errors have been recalculated for the sum with the correlations taken into account. The theoretical prediction for the sum of the branching fractions for $\tau^-\to\nu_\tau\rho^-$, $\tau^-\to\nu_\tau\pi^-2\pi^0$, and $\tau^-\to\nu_\tau\pi^-3\pi^0$ is about 32.0% (Ref. 1) for a τ lifetime of 3.0×10^{-13} s. Therefore, the measured value for $B(\tau^-\to\nu_\tau\pi^-(n\pi^0),n>0)$ is larger than predicted by theory by about $(5.8\pm1.5)\%$. This difference indicates a larger branching fraction to one charged pion plus multiple neutral pions than expected from theoretical predictions, or the presence of other decay modes, such as those with an η in the final state. Limits on the allowed decay modes which include an η are discussed in Appendix A.

D. Conclusions

The leptonic branching fractions measured in this analysis are about one standard deviation higher than the world average of previous measurements[13] and correspond to a τ lifetime of $(3.0\pm0.2)\times10^{-13}$ s which is consistent with the world-average measured τ lifetime. The total branching fraction to one charged hadron plus at least one neutral particle is measured to be $(5.8\pm1.2\pm1.0)\%$ higher than the branching fraction expected from a combination of previous measurements and theoretical predictions.

Unfortunately the errors are too large to identify definitively the source of the discrepancy[1] in the one-prong branching fractions. However, the results suggest that the previously measured leptonic branching fractions may be slightly low and that there exist significant unidentified decay modes which result in one charged hadron and at least one neutral hadron in the final state. In Appendix A, it is shown that the contribution to these final states from decay modes involving the η meson [excluding $\pi^-\eta\pi^0$ from the $\rho(1250)$ resonance or from nonresonant decay] is expected to be less than about 2.4%.

This analysis demonstrates the feasibility of measuring the branching fractions of the τ lepton using a tagging technique and a constrained fit. The main limitation in the analysis is the limited geometrical acceptance and spatial resolution for neutral-particle detection. A similar technique applied to other experiments with large data samples and good electromagnetic calorimetery at e^+e^- storage rings would be helpful in providing further elucidation of the unidentified decay modes.

ACKNOWLEDGMENT

This work was supported by the Department of Energy, Contracts Nos. DE-AC03-76SF00515 (SLAC), DE-AC03-76SF00098 (LBL), and DE-AC02-76ER03064 (Harvard).

APPENDIX A: LIMITS ON DECAY MODES INVOLVING THE η

The possible decay modes with an η in the final state are summarized in Table VIII along with the quantum numbers and possible identity of the resonance. Since the η decays to two charged particles approximately 30% of the time, the decay $\tau^-\to\nu_\tau\pi^-\eta\pi^+\pi^-$ results in five charged particles in the final state 30% of the time and the decay $\tau^-\to\nu_\tau\pi^-\eta\eta$ results in five charged particles 9% of the time. The efficiency for reconstructing these modes as five charged particles is compared to the efficiency for detecting $\tau^-\to\nu_\tau5\pi^\pm\pi^0$ with the final state dis-

TABLE VIII. Possible decay modes with an η in the final state, the corresponding expected resonances and limits on the branching fraction of the τ through this decay mode to final states containing one charged particle.

$\tau^-\to\nu_\tau+$	J^{PG}	Possible resonance	Expected contribution to one-prong branching fraction
$\pi^-\eta\pi^0$	1^{-+}	$\rho(1250)$	No limit
		$\rho(1600)$	0.5%
$\pi^-\eta\pi^+\pi^-$	1^{+-}	A_1	0
$\pi^-\eta\pi^0\pi^0$			$<0.4\%$
$\pi^-\eta\eta$	$0^{--},1^{+-}$	$\pi(1300),A_1$	$<1.5\%$

tributed purely according to phase space which is used in the Mark II measurement of $\tau^- \to \nu_\tau 5\pi^\pm(\pi^0)$ (Ref. 14). The efficiency for detecting the five-prong mode of $\tau^- \to \nu_\tau \pi^- \eta \pi^+ \pi^-$ is the same as for $\tau^- \to \nu_\tau 5\pi^\pm \pi^0$ but the efficiency for detecting the five-prong mode of $\tau^- \to \nu_\tau \pi^- \eta\eta$ is only about half of the efficiency for $\tau^- \to \nu_\tau 5\pi^\pm \pi^0$. Therefore, the measured branching fraction of $(0.14 \pm 0.04)\%$ for $\tau^- \to \nu_\tau 5\pi^\pm(\pi^0)$ (Refs. 14 and 15), can be used to set the following limits:

$$B(\tau^- \to \nu_\tau \pi^- \eta \pi^+ \pi^-) \leq B(\tau^- \to \nu_\tau 5\pi^\pm(\pi^0))/0.3 \approx 0.5\% ,$$

$$B(\tau^- \to \nu_\tau \pi^- \eta\eta) \leq 2B(\tau^- \to \nu_\tau 5\pi^\pm(\pi^0))/0.09 \approx 3.0\% .$$

Also, isospin conservation predicts $B(\tau^- \to \nu_\tau \pi^- \eta \pi^0 \pi^0) \leq B(\tau^- \to \nu_\tau \pi^- \eta \pi^+ \pi^-)$.

A limit can be set on the branching fraction for the mode $\tau^- \to \nu_\tau \pi^- \eta \pi^0$ assuming that it occurs via the $\rho(1600)$ resonance. The branching fraction of the $\rho(1600)$ to $\pi^- \eta \pi^0$ is approximately 7% and to 4π is approximately 60% (Ref. 16). Assuming a total branching fraction of the τ to 4π of 6%, as predicted by Gilman and Rhie,[1] and assuming that all of the 4π decay mode is from the $\rho(1600)$, the branching fraction of the τ to $\nu_\tau \pi^- \eta \pi^0$ through the $\rho(1600)$ resonance is approximately $0.07/0.60 \times 6\%$ which is equal to 0.7%. Since the branching fractions of $\rho(1250)$, the first radial excitation of $\rho(770)$, are not known, a limit cannot be set on the $\nu_\tau \pi^- \eta \pi^0$ final state through the $\rho(1250)$ resonance.

The expected contribution of decay modes involving the η to the branching fraction for final states containing only one charged pion and multiple neutrals is shown in Table VIII. The total contribution excluding $\pi^- \eta \pi^0$ from $\rho(1250)$ and nonresonant decay is expected to be less than 2.4%.

APPENDIX B: SELECTION OF KNOWN LEPTONS IN THE DATA

The lepton rejection efficiencies (for the one-prong tag) and the lepton identification efficiencies (for the tagged sample) are estimated from two sources of known leptons in the data: single-photon production of e^+e^- pairs with initial- or final-state radiation and $\mu^+\mu^-$ pairs with or without initial- or final-state radiation, and two-photon production of e^+e^- and $\mu^+\mu^-$ pairs. The radiative lepton pairs are chosen to provide leptons with a momentum spectrum which extends below 14.5 GeV/c. The radiative sample is obtained by selecting events with two charged tracks and one neutral energy cluster with at least 1 GeV of energy separated from the charged tracks by at least 20 cm in the LA calorimeter. For the electron sample, the two charged tracks project into different LA calorimeter modules. The sum of the momenta of the two charged tracks, as measured by the drift chamber, and the energy of the neutral energy cluster is at least 24 GeV.

The sample of radiative e^+e^- pairs contains an ample number of electron candidates. However, the muon-candidate sample does not have a large number of events. To improve the statistics at high momentum, the muon-candidate sample is supplemented with nonradiative muon pairs. This sample is obtained by selecting events with two charged tracks and no neutral energy clusters of more than 200 MeV. The sum of the momenta of the two charged tracks is greater than 22 GeV/c and less than 36 GeV/c. Information from the TOF system is used to reject cosmic-ray events.

The sample of two-photon-produced events is obtained by selecting events with two charged tracks and no neutral energy clusters of more than 200 MeV. The sum of the momenta of the two charged tracks is less than 12 GeV/c and the net momentum in the event transverse to the beam is less than 300 MeV/c. Again, information from the TOF system is used to reject cosmic-ray events.

For all of the above samples, each charged track is tested with strict lepton-identification criteria. For the nonradiative muon pair sample, the momentum of this track must be between 12 and 16 GeV/c. If a track passes the criteria for an electron (or muon), the other charged track in the event is included in the sample used to check the electron (or muon) rejection efficiency. This results in an unbiased sample of electrons and muons with a small contamination from τ-pair production. The total number of electron candidates is 15 555 and the total number of muon candidates is 4923.

---

[a]Present address: University of California, Santa Cruz, CA 95064.
[b]Present address: University of Pennsylvania, Philadelphia, PA 19104.
[c]Present address: CERN, CH-1211, Genève 23, Switzerland.
[d]Present address: Oxford University, Oxford, England.
[e]Present address: University of Chicago, Chicago, IL 60637.
[f]Present address: Therma-Wave Corporation, Fremont, CA 94539.
[g]Present address: California Institute of Technology, Pasadena, CA 91125.
[h]Present address: Columbia University, New York, NY 10027.
[i]Present address: LPNHE, University Pierre Marie Curie, F-75230 Paris, France.
[j]Present address: Stanford Linear Accelerator Center, Stanford, CA 94305.
[k]Present address: Université de Genève, CH-1211, Genève 4, Switzerland.

[1]F. Gilman and Sun Hong Rhie, Phys. Rev. D **31**, 1066 (1985).

[2]Here we assume that $B(\tau^- \to \nu_\tau \pi^- 2\pi^0)$ is equal to $B(\tau^- \to \nu_\tau \pi^- \pi^+ \pi^-)$ as implied by isospin rules if the 3π state is pure $A(1270)$ resonance, and that $B(\tau^- \to \nu_\tau \pi^- 3\pi^0) = 1.0\%$ which is the result of using the conserved-vector-current hypothesis and e^+e^- cross-section measurements to 4π final states. See Ref. 1 for more details.

[3]At a center-of-mass energy of 29 GeV, the decay products of one τ are easily separated from the decay products of the other τ in the pair.

[4]For a detailed description, see P. R. Burchat, Ph.D. thesis, Report No. SLAC-292, 1986.

[5]For a detailed description see M. E. Nelson, Ph.D. thesis, Report No. LBL-16724, 1983 (unpublished).

[6]F. James and M. Roos, Comput. Phys. Commun. **10**, 343 (1975).
[7]F. A. Berends and R. Kleiss, Nucl. Phys. **B177**, 239 (1981).
[8]R. L. Ford and W. R. Nelson, Report No. SLAC-PUB-2107, 1978 (unpublished).
[9]W. B. Schmidke, internal Mark II memo, November, 1985 (unpublished).
[10]G. B. Mills *et al.*, Phys. Rev. Lett. **52**, 1944 (1984).
[11]J. M. Yelton *et al.*, Phys. Rev. Lett. **56**, 812 (1986).
[12]W. B. Schmidke *et al.*, Phys. Rev. Lett. **57**, 527 (1986).
[13]For recent reviews of the properties of the τ and references to specific experiments see Ref. 4 and K. K. Gan, in *Proceedings of the Oregon Meeting*, proceedings of the 1985 Annual Meeting of the Division of Particles and Fields of the APS, Eugene, Oregon, 1985, edited by R. C. Hwa (World Scientific, Singapore, 1985), p. 248.
[14]P. R. Burchat *et al.*, Phys. Rev. Lett. **54**, 2489 (1985).
[15]M. Derrick *et al.*, Phys. Rev. Lett. **54**, 1775 (1985).
[16]Particle Data Group, Rev. Mod. Phys. **56**, S1 (1984).